

Special  
Collection

# Rebound or Cage Escape? The Role of the Rebound Barrier for the Reactivity of Non-Heme High-Valent Fe<sup>IV</sup>=O species

Ravi Kumar,<sup>[a]</sup> Azaj Ansari,<sup>[b]</sup> Peter Comba,<sup>\*,[c]</sup> and Gopalan Rajaraman<sup>\*,[a]</sup>

Owing to their high reactivity and selectivity, variations in the spin ground state and a range of possible pathways, high-valent Fe<sup>IV</sup>=O species are popular models with potential bioinspired applications. An interesting example of a structure–reactivity pattern is the detailed study with five nonheme amine-pyridine pentadentate ligand Fe<sup>IV</sup>=O species, including N4py: [(L<sup>1</sup>)Fe<sup>IV</sup>=O]<sup>2+</sup> (1), bntpen: [(L<sup>2</sup>)Fe<sup>IV</sup>=O]<sup>2+</sup> (2), py<sub>2</sub>tacn: [(L<sup>3</sup>)Fe<sup>IV</sup>=O]<sup>2+</sup> (3), and two isomeric bispidine derivatives: [(L<sup>4</sup>)Fe<sup>IV</sup>=O]<sup>2+</sup> (4) and [(L<sup>5</sup>)Fe<sup>IV</sup>=O]<sup>2+</sup> (5). In this set, the order of increasing reactivity in the hydroxylation of cyclohexane differs from that with cyclohexadiene as substrate. A comprehensive DFT, ab initio

CASSCF/NEVPT2 and DLPNO-CCSD(T) study is presented to untangle the observed patterns. These are well reproduced when both activation barriers for the C–H abstraction and the OH rebound are taken into account. An MO, NBO and deformation energy analysis reveals the importance of  $\pi(\text{pyr}) \rightarrow \pi_{xz}^*(\text{Fe}^{\text{III}}\text{-OH})$  electron donation for weakening the Fe<sup>III</sup>-OH bond and thus reducing the rebound barrier. This requires that pyridine rings are oriented perpendicularly to the Fe<sup>III</sup>-OH bond and this is a subtle but crucial point in ligand design for non-heme iron alkane hydroxylation.

## Introduction

High-valent metal intermediates such as oxido, peroxido, hydroperoxido and superoxido species act as reactive intermediates in catalytic reactions in biology and industrial processes. Several important enzymes, including TauD, CytC3, SyrB2, phenylalanine hydrolase, prolyl-4-hydroxylase and tyrosine hydroxylase contain terminal Fe<sup>IV</sup>=O species at their catalytically active site.<sup>[1–9]</sup> These and other non-heme iron proteins perform various transformations, including dehydrogenation, halogenation, hydroxylation and olefin epoxidation.<sup>[10]</sup> Especially C–H and C=C bond activation are important in both biological and industrial processes.<sup>[11]</sup>

In the last two decades, numerous biomimetic Fe<sup>IV</sup>=O species were synthesized and studied in great detail to understand fundamental structural, functional and mechanistic aspects and their interrelation in enzymes and bioinspired oxidation catalysts.<sup>[12–15]</sup> Low molecular weight model chemistry allows to systematically tune the reactivity and product selectivity of oxygen activation based processes. Various ligand architectures, enforcing specific geometries and electronic properties, were found to enable enhanced (or diminished) reactivities of Fe<sup>IV</sup>=O species. For example, the Fe<sup>IV</sup>=O complex [(L<sup>NHC</sup>)(CH<sub>3</sub>CN)Fe<sup>IV</sup>=O]<sup>2+</sup> with the cyclic tetracarbene ligand L<sup>NHC</sup> (L<sup>NHC</sup> = 3,9,14,20-tetraaza-1,6,12,17-tetraazoniapentacyclohexacosane-1(23),4,6(26),10,12(25),15,17(24),21-octaene) is a sluggish oxidant and activates only weak C–H bonds such as those of 9-H-xanthane with a second order rate constant of 2.2 M<sup>-1</sup> s<sup>-1</sup>,<sup>[16–18]</sup> while the structurally similar heme oxidant [(4-TMPyP<sup>+</sup>)(H<sub>2</sub>O)Fe<sup>IV</sup>=O] (4-TMPyP = 5,10,15,20-tetrakis(*N*-methyl-4-pyridinium)porphyrin) is extremely reactive and activates the same substrate with a second order rate constant of 3.6 · 10<sup>6</sup> M<sup>-1</sup> s<sup>-1</sup> and also activates the very strong C–H bonds of cyclohexane and ethylbenzene.<sup>[19]</sup> The most reactive non-heme iron oxidant known to date is based on a tetradentate bispidine ligand (bispidine = 3,7-diazabicyclo[3.3.1]nonane) and its second order rate constant with cyclohexane as substrate is 7.6 · 10<sup>2</sup> M<sup>-1</sup> s<sup>-1</sup> at –90 °C, i.e. it has a reactivity of the order of enzymes.<sup>[20,21]</sup>

The design of efficient catalysts requires a thorough understanding of the reaction mechanism, and often computational tools are required to complement experimental data. Ferryl oxidants generally occur in two electronic ground states, S = 1 and S = 2 (triplet and quintet), and, in contrast to enzymes, the systems with pentadentate amine-pyridine ligands discussed here (see Scheme 1) all have triplet ground states. The hydroxylation of alkane substrates is a two-step procedure with the C–H abstraction followed by a rebound step (see

[a] R. Kumar, G. Rajaraman  
Department of Chemistry  
Indian Institute of Technology Bombay  
Mumbai, Powai-400076 (India)  
E-mail: rajaraman@chem.iitb.ac.in

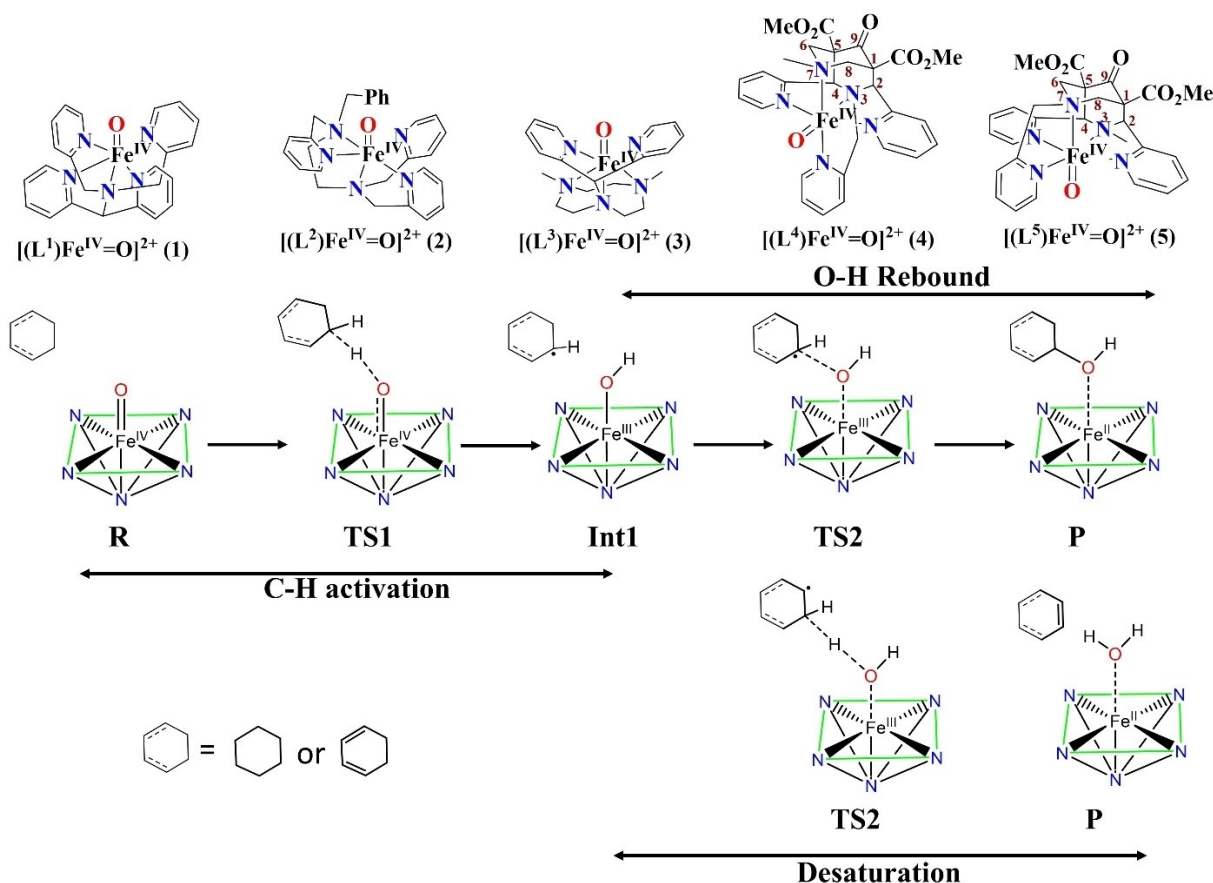
[b] A. Ansari  
Department of Chemistry  
Central University of Haryana  
Haryana-123031 (India)

[c] P. Comba  
Institute of Inorganic Chemistry &  
Interdisciplinary Center for Scientific Computing  
Heidelberg University  
69120 Heidelberg (Germany)  
E-mail: peter.comba@aci.uni-heidelberg.de

Supporting information for this article is available on the WWW under <https://doi.org/10.1002/chem.202303300>

This article is part of a joint Special Collection dedicated to Roger Alberto.

© 2023 The Authors. Chemistry - A European Journal published by Wiley-VCH GmbH. This is an open access article under the terms of the Creative Commons Attribution Non-Commercial NoDerivs License, which permits use and distribution in any medium, provided the original work is properly cited, the use is non-commercial and no modifications or adaptations are made.



**Scheme 1.** Schematic representation of the  $Fe^{IV}=O$  complexes discussed in this work and the general mechanism adapted for cyclohexane hydroxylation (C–H activation + O–H rebound) and cyclohexadiene (CHD) desaturation (C–H activation, desaturation, i.e., a  $2e^-/2H^+$  process).

Scheme 1), where the hydrogen atom abstraction (HAA) generally is believed to be rate determining.<sup>[22,23]</sup> An important parameter, therefore is the oxidation power of the ferryl species, *i.e.* the driving force, which according to the Bell–Evans–Polanyi principle, is correlated to the activation barrier.<sup>[24,25]</sup> Unfortunately, accurate and reliable experimental and computational data for redox potentials of  $Fe^{IV}=O$  is scarce.<sup>[26–33]</sup> The approaches used involve cyclic voltammetry in dry acetonitrile, aqueous acetonitrile or pure water,<sup>[27,28]</sup> titrations of the  $Fe^{IV}=O$  complexes in acetonitrile with ferrocene derivatives with known redox potentials to determine the ferrocene/ferrocenyl and the corresponding  $Fe^{IV}=O/Fe^{III}-O$  equilibria,<sup>[29,30,34]</sup> and spectrophotometric titrations of the iron(III)-hydroxido complexes in wet acetonitrile (PCET potential).<sup>[26,27]</sup> Apart from the latter approach, which does not allow to obtain the potential of the electron transfer but rather that of PCET (which is relevant for HAA but depends on the substrate), the methods involve the equilibrium between  $Fe^{IV}=O$  and  $Fe^{III}-O$  with the caveat that  $Fe^{III}-O$  generally is unstable,<sup>[31]</sup> and there is only one known isolated and fully characterized  $Fe^{III}-O$  complex.<sup>35</sup> A number of computational approaches have been proposed but most suffer from the problem that the error margins of the computed energies are too large and lead to errors in redox potentials in the 100 mV area.<sup>[32,33]</sup>

The other parameter of importance for the reactivity of the oxidant for C–H activation is the spin ground state of the ferryl oxidant. In general, the HAA proceeds over a high-spin transition state, and with  $S=1$   $Fe^{IV}=O$  species two-state or multi-state reactivity generally is evoked, and the ease of spin crossover depends primarily on the triplet–quintet gap and the spin–orbit coupling.<sup>[21,36]</sup> Generally, density functional theory methods (DFT) are employed with a suitable exchange–correlation functional (often B3LYP) to probe mechanistic aspects of  $Fe^{IV}=O$  initiated reactions. However, although DFT generally yields reasonably accurate geometries and energies, it often fails to predict the correct spin ground state.<sup>[37–40]</sup> While high-level quantum-chemical methods such as coupled cluster single-double and perturbative triple [CCSD(T)] are very robust, the high computational cost, particularly at the basis set limit, makes them unavailable for systems of the size discussed here.<sup>[41,42]</sup> New developments, especially domain-based local pair natural orbital-CCSD(T) [DLPNO-CCSD(T)] methods, allow to circumvent this problem but obviously also have limitations (see below).<sup>[43–45]</sup>

The set of ferryl complexes with the pentadentate amine-pyridine ligands  $L^1$ – $L^5$  discussed here (see Scheme 1) has been studied in detail experimentally (optical, vibrational, XAS spectroscopies, electrochemistry, reactivities with various substrates),<sup>[26]</sup> and some of the relevant data are given in

Table 1, where computational parameters discussed below are also included (tabulated in italics; see Supporting Information for more computational and experimental data, Table S1). An interesting observation is that the orders of reactivities with cyclohexane and cyclohexadiene as substrate are strikingly different: the bispidine complex **5** is by far the most reactive with cyclohexane, while the bntpen complex **2** is somewhat faster than **5** with cyclohexadiene. While the cyclohexyl radical/ $\text{Fe}^{\text{III}}\text{-OH}$  intermediate (Int1 in Scheme 1) generally reacts via a rebound pathway to the alcohol product (with competing cage escape that can become dominant with a large rebound energy barrier, TS2 in Scheme 1),<sup>[23,46,47,48]</sup> the cyclohexadienyl radical/ $\text{Fe}^{\text{III}}\text{-OH}$  intermediate reacts with a fast second HAA to benzene (desaturation). Here, we therefore carefully analyze the electronic structures of the five ferryl complexes 1–5 as well as those of the corresponding ferric hydroxido species with state-of-the-art DFT and various ab initio methods including CASSCF/NEVPT2/ICE-Cl (complete active space selfconsistent field) and DLPNO-CCSD(T).

## Computational Details

All calculations were carried out with Gaussian 09 and ORCA 4.0.1.<sup>[50,51]</sup> The geometries were optimized using Grimme's dispersion corrected unrestricted B3LYP functional.<sup>[52,53]</sup> Two different basic sets were used; iron is described with the Lan2DZ effective core basis set, and 6-31G is used for N, H, C, and O. Frequency calculations were performed to obtain a single negative frequency (imaginary frequency). All energies discussed are relative Gibbs free energies, including the Gibbs free energy correction. The solvation energies have been computed using the polarisable continuum model (PCM),<sup>[54]</sup> employing acetonitrile as the solvent with a TZVP triple zeta basis set. Here, the level of theory used is B3LYP-D2/TZVP//B3LYP-D2/Lan2DZ(Fe),6-31G(C, H, N, O) (BS1). We have performed further calculations using B3LYP-D3/TZVP//B3LYP-D3/Lan2DZ(Fe),6-31G\*(C, H, N, O) (BS2) to understand the effect of polarisation and dispersion on the results, and both BS1 and BS2 yield similar results (see Table S6 in the Supporting Information); in the text, we primarily discuss the results obtained with BS1.

In order to gain confidence in the computed energetics, we have also performed ab initio calculations using CASSCF/NEVPT2/ICE-Cl and DLPNO-CCSD(T) implemented in ORCA, employing DFT optimized geometries.<sup>[51]</sup> The multiconfigurational calculations<sup>[55–57]</sup> based on state-averaged complete active space self-consistent field (SA-CASSCF), followed by *N*-electron valence perturbation theory of second-order (NEVPT2)<sup>[58,59]</sup> were performed at CAS(4,5) and expanded to CAS(12,14) using the def2-TZVP basis set. The CAS(12,14) active space consists of five iron 3d orbitals, three oxygen p-orbitals, the bonding counterpart of the iron  $d_{x^2-y^2}$  orbital, and five empty iron 4d-orbitals to include the double-shell effect.<sup>[17,60,61]</sup> Here, relativistic effects are included via Douglas–Kroll–Hess (DKH) Hamiltonians with DKH-def2-TZVP for Fe, DKH-def2-TZVP(–f) for N, O, and DKH-def2-SVP for all other atoms.<sup>[62]</sup> More than 14 orbitals can be treated using the iterative-configuration expansion configuration interaction (ICE-Cl) in ORCA and were performed with 14 electrons in 16 orbitals (14e,16o).<sup>[63,64,65]</sup> The domain-based local pair natural orbital coupled cluster approach with singles, doubles and perturbative triples (DLPNO-CCSD(T)), which was shown to yield good numerical accuracy for spin-state energetics, has been used to estimate energies, employing DFT geometries.<sup>[43,66–69,70]</sup> Benchmarking with various basis sets and other recommended criteria, cc-PVTZ, TIGHTPNO, and NO Frozen core were used to obtain optimal results (see Supporting Information, Table S2 for the full analysis).<sup>[71–73]</sup>

## Results and Discussion

### Electronic Structure of Complexes 1–5

DFT calculations in general suffer from the problem not to be able to accurately describe metal ligand bonding and in particular to accurately compute spin state energetics.<sup>[37,38,40]</sup> The setup used here is believed to be a reasonable compromise for the description of the ground state and spin gaps of the ferryl reactant as well as the transition states of the HAA and the rebound steps. One also needs to be careful in the interpretation of the energy barriers, and generally accepted error limits are of the order of approx. 10–15 kJ/mol.<sup>[74–76]</sup> Ab

**Table 1.** Experimental and computed kinetic, thermodynamic and vibrational spectroscopic data of the iron(IV)-oxido compounds 1–5, ordered as a function of the reactivity with cyclohexane as substrate (trivial names of the ligands are also given for convenience); computed data are in italics; the experimental data are from literature.<sup>[13,26,29,34,49]</sup> An extended version of this Table is available in the Supporting Information (Table S1).

complex	C–H activation ( $k_2$ [ $\text{M}^{-1}\text{s}^{-1}$ ]) <sup>[d]</sup>			redox potential [V vs. $\text{Fc}^{+/0}$ ] <sup>[h]</sup>				
	cyclohexane <sup>[d]</sup>			cyclohexadiene <sup>[e]</sup>				
	exp	<i>TS1</i>	<i>TS2</i> <sup>[f]</sup>	exp	<i>TS1</i>	PCET <sup>exp</sup>	<i>PCET</i> <sup>calc</sup>	<i>ET</i> <sup>calc</sup>
<b>5</b> bisp-b	$4.9 \cdot 10^{-3}$	78.6	0.0 <sup>[g]</sup>	0.37	17.0	1.23	1.27 <sup>[b]</sup>	1.52
<b>2</b> bntpen	$3.9 \cdot 10^{-4}$	75.1	35.7	0.96	16.8	1.07	1.09	1.46
<b>4</b> bisp-a	$1.3 \cdot 10^{-4}$	82.8	52.7	0.014	24.9	(0.98) <sup>[a]</sup>	0.96	1.44
<b>1</b> N4py	$5.5 \cdot 10^{-5}$	87.0	57.4	0.07	24.5	0.90	0.95	1.16
<b>3</b> py <sub>2</sub> tacn	n.r.	86.7	95.4	0.027	35.7	0.83	0.87	0.92

[a] This value is estimated based on the  $E_{\text{PCET}}$  vs.  $E_{1/2}(\text{IV/III})$  correlation in Ref. [26]. [b] All computed PCET potentials ( $\text{Fe}^{\text{IV}}=\text{O}/\text{Fe}^{\text{III}}\text{-OH}$ ) are at pH=4, except for **5**, where the computed value at pH=0 is 1.27 V and at pH=4 is 1.03 V; see Supporting Information for the computational procedures for the redox potentials (Schemes S1–S3, Table S12). [c] Comparison of the experimental  $k_2$  values ( $\text{M}^{-1}\text{s}^{-1}$ ) with the computed barrier heights ( $\text{kJmol}^{-1}$ ). [d] For cyclohexane, the  $k_2$  values (measured in MeCN at 298 K) are taken from Ref. [13] and Ref. [34]. [e] For cyclohexadiene, the  $k_2$  values (measured in MeCN at 233 K) are taken from Ref. [26]. [f] Rebound barrier (TS2). [g] Barrierless. [h] The PCET potentials are from Ref. [26]. ET potentials are problematic; published values<sup>[29,34]</sup> are given the Supporting Information, Table S1.

initio calculations with acceptable computational expense that have been used here to support the DFT calculations include CASSCF/NEVPT2, which bears the problem of an inadequate treatment of dynamic correlation, and DLPNO-CCSD(T), a single reference method. While these approaches obviously also have limitations and lead to results that need to be interpreted with caution,<sup>[45,77–79]</sup> the combination of the various methods as well as benchmarking add to the reliability. Importantly, we consider a series of five similar systems, where differences in the energy barriers and triplet–quintet gaps rather than absolute values are of importance and where these differences are correlated with published experimental data.

The DFT calculations yield  $S=1$  as the ground state with triplet–quintet gaps in the order of 10 to 25 kJ/mol (see Supporting Information, Table S2). CASSCF calculations predict  $S=2$  as the ground state with  $S=1$  strongly destabilized with the minimal reference space (CAS(4,5)SCF), and NEVPT2 diminishes the gap substantially (Table S2). Expansion of the CAS reference space to CASSCF(12,14) with the inclusion of dynamic correlation reduces the gap further to values similar to those of the DFT calculations (Table S2, Figure S1). Since an additional expansion of the reference space was not practical, the ICE-Cl approach with a (14e,16o) reference<sup>[65]</sup> was used and yielded an  $S=2$  ground state with the triplet state at around 30 kJ/mol (Table S2). Considering the importance of a reference space expansion, we have turned to the single reference method DLPNO-CCSD(T), which in a number of examples led to the correct prediction of the spin ground state of ferryl complexes (see Supporting Information, Table S2 for a limited benchmarking; set-up used: DLPNO-CCSD(T)/cc-pVTZ: TightPNO/No FC).<sup>[45,70,77–79]</sup> The predicted  $S=1$  ground states are in agreement

with the experiment and the triplet–quintet gaps are in remarkably good agreement with the DFT results (1–5, DLPNO/DFT (kJ/mol): 20/25, 4/7, 20/22, 17/20, 14/18, Table S2, Figure S2).<sup>[26]</sup>

The Fe–O bond distances in the  $S=1$  and  $S=2$  states are in the expected range of 1.650–1.654 Å and 1.642–1.646 Å, respectively (see Figure 1a and Table S3). The Fe–N distances (Fe–N<sub>ax</sub> and average Fe–N<sub>eqr</sub> triplet ground state) are found to vary in the range of 1.978 Å to 2.119 Å. The Fe–N<sub>ax</sub> distances for 2 and 5 are significantly different from the others, and these two complexes are the most reactive in the entire set, suggesting that the ligand-enforced structural distortion may contribute to the reactivity (see below).<sup>[34]</sup>

The ground state electronic configuration for all complexes is  $(\delta_{xy})^2(\pi^*_{xz})^1(\pi^*_{yz})^1(\sigma^*_{x-y})^0(\sigma^*_{z^2})^0$  (see Table S4). For the favorable and generally observed  $\sigma$  pathway of the HAA step, the relative energy of the  $\sigma^*_{z^2}$  orbital at the  $S=2$  state is determinantal for the reactivity (see above for the spin gaps and structural effects and below for the reactivity). State-average CASSCF/NEVPT2 calculations on the  $S=1$  ground state are used to understand the multiconfigurational character of the Fe<sup>IV</sup>=O centers 1–5. The results (see Table S4) suggest dominant triplet ground states (approx. 75%) with little mixing of the excited state triplet for 1, 3 and 4. For the more reactive species 2 and 5, there is significantly stronger mixing of the ground state configuration  $(\delta_{xy})^1(\pi^*_{xz})^1(\pi^*_{yz})^1(\sigma^*_{x-y})^0(\sigma^*_{z^2})^0$  (51% and 42%, 2, 5) with excited state triplet configurations  $(\delta_{xy})^1(\pi^*_{xz})^1(\pi^*_{yz})^0(\sigma^*_{x-y})^1(\sigma^*_{z^2})^0$  (22%, 2) and  $(\delta_{xy})^1(\pi^*_{xz})^1(\pi^*_{yz})^0(\sigma^*_{x-y})^0(\sigma^*_{z^2})^1$  (13%, 5, see Table S4). The stronger mixing in 2 and 5 suggests a correlation of the multireference character with reactivity, and the ratio of mixing follows the reactivity pattern (see below), i.e.

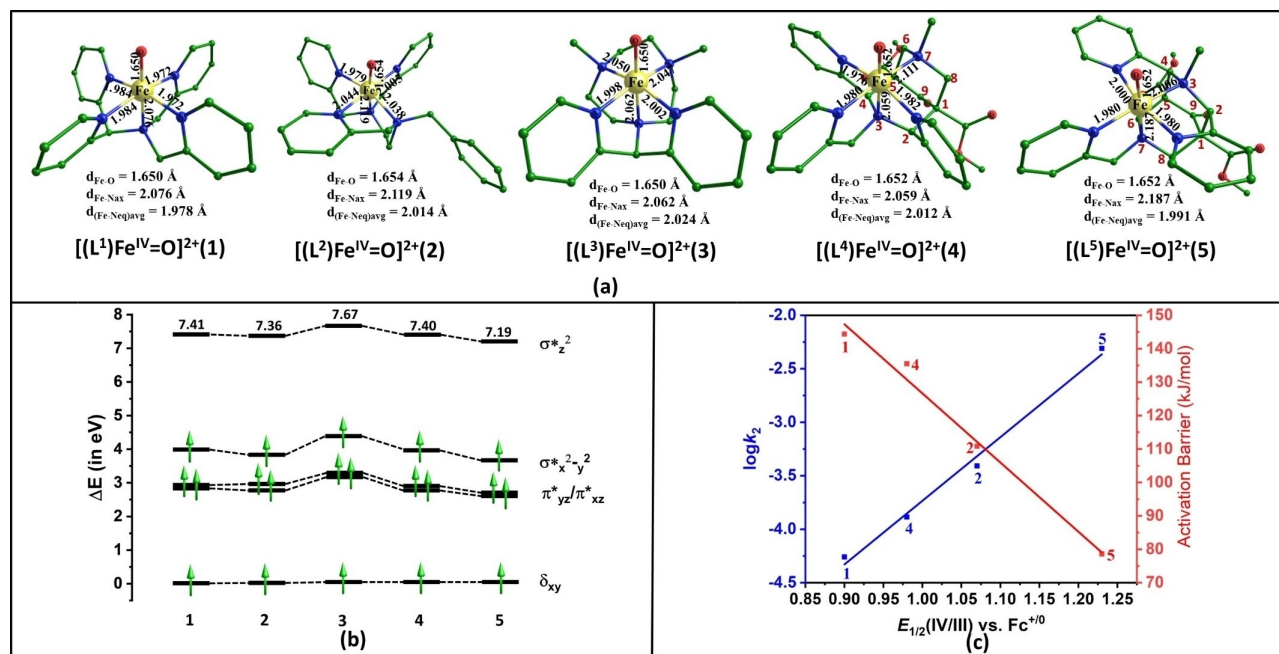


**Figure 1.** (a) DFT computed ground state structures of the Fe<sup>IV</sup>=O complexes 1–5, (b) orbital energy diagram of the DFT computed  $S=2$  state of 1–5, (c) plots of  $\log k_2$  (left, experimental data) and DFT computed HAA activation barriers (right) for the oxidation of cyclohexane (298 K, CH<sub>3</sub>CN) vs. the  $E_{1/2}^{\text{PCET}}$  (V vs. Fc, experimental data, see Table 1).<sup>[26]</sup>

these calculations are an interesting tool for probing the reactivity of high-valent metal-oxido species.<sup>[80]</sup>

### Reactivity of Complexes 1–5

The conversion of cyclohexane to cyclohexanol and that of cyclohexadiene to benzene are initiated by a HAA, which generally is believed to be rate limiting. For cyclohexane as substrate, the observed second-order rate constants ( $k_2$ ) decrease from **5** to **2** to **4** and to **1** by factors of over 10 to 2 per step, and **3** does not react at all with cyclohexane at 298 K (see Table 1).<sup>[13,34]</sup> According to the Bell–Evans–Polanyi principle the rate should be correlated to  $\Delta G$  of the HAA (i.e. the potential of the PCET),<sup>[24,25]</sup> and this clearly is the case when comparing the corresponding rows of the experimental data in Table 1 (see also Figure 1c). With cyclohexadiene, the reactions are significantly faster (as expected from the smaller C–H bond dissociation energies), with a slightly different order: **2** is faster than **5** (factor of 2.5), and the set the other three  $\text{Fe}^{\text{IV}}=\text{O}$  species **1**, **3** and **4** are approx. 10-fold slower oxidants with similar reactivities, and the order is slightly different than for cyclohexane (see Table 1). Redox potentials for ferryl complexes are notoriously problematic, both in terms of experiments and computational work (see Introduction). Relevant for the HAA processes discussed here are the potentials of the PCET, and these have been determined experimentally for **1**, **2**, **3** and **5** (for **4** it was not possible to determine a potential, and the tabulated value is merely obtained from a correlation with kinetic data).<sup>[26]</sup> Computation of redox potentials has been done with moderate success by simple empirical correlations as well as by quantum-chemically based methods<sup>[32, 33, 81]</sup> – for the ferryl oxidants discussed here, problems include the definition of the spin ground states and the accuracy of energetics in general, as well as solvation and entropy effects. A major problem is that an error margin of the computational method of approx. 10 kJ/mol translates to a substantial error of 100 mV in the computed potential. The computed values of the redox potentials, based on DFT data from square schemes for **1** to **5** are given in Table 1.<sup>[82]</sup> Details of the calculations of the redox potentials as well as the potentials of the PCET are given in the Supporting Information (Schemes S1–S3, Table S12; this also includes thermodynamic cycles for the oxidants 1–5 with cyclohexane; also included in Table S12 are computed  $\text{p}K_{\text{a}}$  values of catalysts 1–5 as well as of their one-electron-reduced forms [ $\text{Fe}^{\text{III}}\text{-OH}/\text{Fe}^{\text{III}}\text{-O}$ ]). As seen from the thermodynamic cycles, as expected, the PCET pathway is favored for all oxidants 1–5, with high penalties for stepwise PT-ET or ET-PT mechanisms. The individual  $\text{p}K_{\text{a}}$  values are in the expected ranges for  $\text{Fe}^{\text{IV}}=\text{OH}$  and  $\text{Fe}^{\text{III}}\text{-OH}$  but the limited accuracy and the relatively small differences between the five ligand systems considered do not suggest that the reactivities can be correlated to differences in proton affinities either in the oxidized or reduced form.<sup>[83–85]</sup>

The hydroxylation of cyclohexane involves a HAA followed by the radical rebound, and this has been computed by DFT and also in combination with DLPNO-CCSD(T), and preliminary calculations have also been made with cyclohexadiene as

substrate (see Scheme 1 and Table 1). For all five iron(IV)-oxido complexes and for both substrates, HAA (*TS1*) follows the  $\sigma$ -pathway on the quintet and the  $\pi$ -pathway on the triplet spin surface (see Figures S3, S5 and S6).<sup>[42]</sup> The computed activation barriers for cyclohexane are given in Table 1 and Figure 2, for more details see the Supporting Information (Figure S4). DFT predicts for **1** and **2** a slightly lower energy barrier on the triplet surface, while all other reactions are, as generally expected, computed to occur over a quintet transition state. The DLPNO-CCSD(T) calculations predict a lower barrier on the quintet surface for all five ferryl species, consistent with the established reactivity pattern observed for  $\text{Fe}^{\text{IV}}=\text{O}$  species in general (see Table S5).<sup>[15,42,61,80,86,87]</sup> The hydrogen atom abstraction leads to the formation of the  $\text{Fe}^{\text{III}}\text{-OH}/\text{cyclohexyl}$  radical intermediate (*1-Int1*) with a quintet ground state ( $S=5/2$  on the  $\text{Fe}^{\text{III}}$  center and a spin-down cyclohexyl radical), with the triplet state lying higher in energy by 1–23 kJ/mol (see Supporting Information, Table S3). Formation of the  $\text{Fe}^{\text{III}}\text{-OH}/\text{cyclohexyl}$  radical intermediate is endothermic by 5–33 kJ/mol, with the unreactive oxidant **3** as the thermodynamically least favorable oxidant, see Figure 2. Based on the DLPNO calculated energies, the OH rebound step via *TS2* stays on the quintet surface, except for **3** with an exceedingly high barrier and **5**, which is assumed to have a barrierless rebound (see Figure 2 and Supporting Information; the interpretation that the rebound step is barrierless for **5** is supported by a relaxed scan, see Supporting Information, Figure S7). Figure 2 also shows that the overall exothermicity is largest for the most reactive of all complexes studied here, i.e. that with a bispidine ligand scaffold.

While for all five complexes, the C–H bond activation occurs on the  $\sigma$ -pathway the rebound step occurs on a  $\pi$ -channel. Since all  $\text{Fe}^{\text{IV}}=\text{O}$  complexes have a triplet ground state and the lowest HAA transition state energies corresponding to quintet states, one expects a spin-transition along the reaction pathway, suggesting two-state reactivity in the C–H bond activation step. To better understand the observed reactivity pattern, the C–H bond activation barrier was analyzed in detail. Independently of the level of theory, the HAA barriers for the five ferryl oxidants are in a very narrow range (10–20 kJ/mol, translating to an approx. 15 to 30-fold rate increase from the slowest to the fastest of the five oxidants), and this does not account for the observed acceleration of 2 to 3 orders of magnitude (see Table 1).

The rebound barriers (see Figure 2, Table 1) suggest a rebound reactivity order of  $5 > 2 > 4 > 1 > 3$ , exactly matching the experimental rate constants. Specifically, the rebound barrier of the  $\text{py}_2\text{tacn}$ -based species **3** of around 100 kJ/mol [95.4 kJ/mol DFT, 111.4 kJ/mol DLPNO-CCSD(T)] agrees with the experimentally observed lack of reaction – the rebound barrier is around 10 kJ/mol higher than that of the HAA. As the overall reaction has more than one significant energy barrier and as even the rate-limiting step varies in the series of oxidants under consideration, the sum of the two barriers (CB: combined barrier, i.e. barrier of [*TS1*] + barrier of [*TS2*]) might be useful to understand the hydroxylation reactivity of the five oxidants and possibly is more appropriate than the usually discussed barrier of the (rate-determining) HAA step.<sup>[88]</sup> The values of CB for the

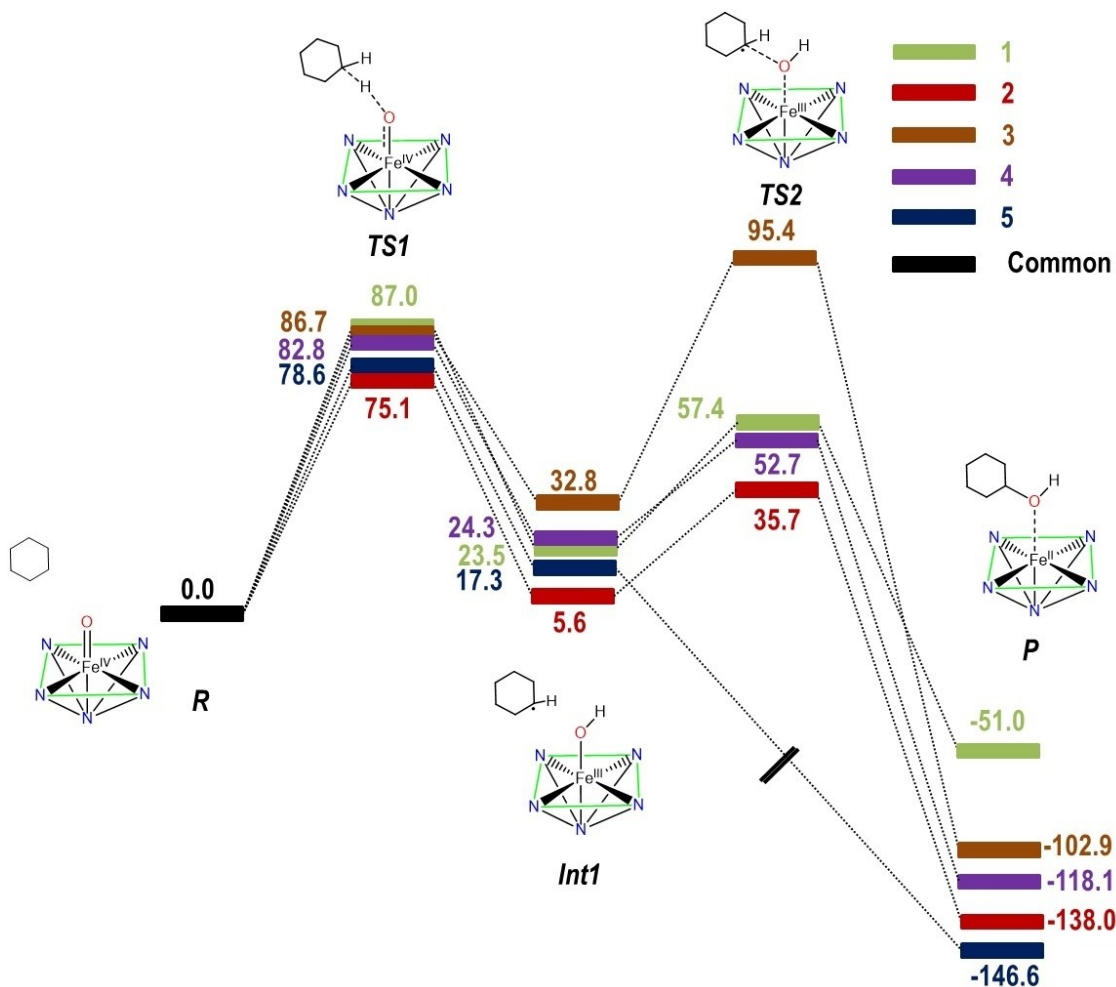


Figure 2. Comparative energy profile diagram ( $\Delta G$  in kJ/mol, B3LYP-D2) for the low-lying energy surface of 1–5.

oxidation of cyclohexane by 1–5 are estimated to be 144.4 (DLPNO 135.4), 110.8 (123.9), 182.1 (110.7), 135.5 (138.5), and 78.6 (60.3) kJ/mol, and this correctly correlates with the observed reactivities of  $5 > 2 > 4 > 1 > 3$  (see Table S7). Note however that, while the relative barrier heights of parallel pathways involving a short-lived intermediate after a rate-limiting initial step can be directly correlated to the product distributions, the use of CB for a correlation with kinetic parameters can be an oversimplification and has to be considered with caution. In addition, for both reactions (cyclohexane and cyclohexadiene as substrate), there are three pathways for the decay of the  $\text{Fe}^{\text{III}}\text{-OH}$ /radical Int1, i.e., rebound, cage escape and desaturation (due to aromatization the latter is assumed to be the major route for cyclohexadiene but here we are mainly focusing on cyclohexane).

For HAA at cyclohexane with the N4py and bntpen based ferryl oxidants 1 and 2 experimental and DFT-based evidence for a mechanism based on cage escape (radical diffusion pathways) to produce iron(III) species and cyclohexanol, cyclohexanone, cyclohexene as well as bromocyclohexane (depending on the reaction conditions) as organic products has been discussed.<sup>[23,47]</sup> Cage escape for various ferryl-based oxidations

has also been discussed some time ago based on the comparison of reactions under inert atmosphere and reactions in presence of dioxygen, also involving  $^{18}\text{O}$  labeling studies.<sup>[49,89–92]</sup> We therefore have also computed cage escape/radical diffusion pathways (see Supporting Information, Table S11).<sup>[93]</sup> The corresponding cage escape energies for the oxidants 1–5 are  $-38.7$ ,  $-37.3$ ,  $-47.8$ ,  $-35.1$  and  $-28.1$  kJ/mol, respectively, i.e., exothermic but with much smaller energies than the rebound products. Apart from 5 with a barrierless rebound process and 3, which does not react with cyclohexane, rebound and cage escape products are predicted to be formed, and for 1 and 2<sup>[47]</sup> as well as for 4<sup>[49]</sup> this is supported by experimental data; the published relative energies of 1 and 2 at different levels of theory are comparable to those reported here (Figure 2, Table S11).<sup>[23,47]</sup> However, while cage escape is an obvious pathway in nonheme iron model systems, supported by experiment (and by computational modeling) in a number of examples, it would be an overinterpretation and unnecessary oversimplification to assume that cage escape is the general and sole pathway. An important example to support this is the HAA reaction with cyclohexane as substrate and a chloro-ferryl oxidant with a tetradentate bispidine ligand that selectively

produces chlorocyclohexane in high yield, where it was shown unambiguously that the product results from a rebound process.<sup>[48]</sup>

As there is a significant variation in the rebound barriers for all five oxidants studied here, the electronics of this step was carefully analyzed. Since no barrier was found for the hydroxide species of **5**, the electronic structures of the Fe<sup>III</sup>-OH intermediates were studied in detail. The Fe<sup>III</sup>-OH distances in **1–5** increase from **3** (1.781 Å) to **1** (1.788 Å), **4** (1.791 Å), **2** (1.798 Å) and **5** (1.803 Å), and this follows the trend of increasing reactivity. To understand the origin of the difference in the Fe<sup>III</sup>-OH bond lengths, the frontier molecular orbitals (MO) of the Fe<sup>III</sup>-OH species were analyzed. Two pyridine  $\pi$  MOs (i.e., those perpendicular to the Fe<sup>III</sup>-OH bond) make a strong donation to the  $\pi^*_{xz}(\text{Fe-OH})$  orbitals in **5**, while there is no such effect in **3** because **3** does not have any pyridine donor perpendicular to the Fe<sup>III</sup>-OH bond (there are none in **1**, **3** and **4**, **1** in **2** and **2** in **5**). The donation into the antibonding  $\pi^*_{xz}(\text{Fe-OH})$  orbital weakens the Fe<sup>III</sup>-OH bond, leading to significant elongation (1.781 Å vs. 1.803 Å for **3** and **5**, see Figure 3; 1.788, 1.798, 1.791 Å for **1**, **2**, **4**, respectively). The elongation of Fe<sup>III</sup>-OH leads to a reduction of the rebound barrier as the cyclohexyl radical encounters less steric strain and hence better orbital overlap with the OH-Fe<sup>III</sup> partner. This is reflected in the computed deformation energies of *TS2* (81.5 kJ/mol for **3** vs. 4.5 kJ/mol for **2** (since the rebound for **5** is barrierless, the comparison is made with the second most reactive species; see Figure S7 and Table S9 in the Supporting Information). The effect of perpendicular pyridine donors is also supported by a quantitative NBO donor-acceptor interaction analysis performed for the Fe<sup>III</sup>-OH intermediates (see Supporting Information, Table S8). This reveals that, due to variation in the acceptor orbitals, the Fe<sup>III</sup>-

OH bond in **3** is significantly stronger (107.5 kJ/mol) than in **5** (20.5 kJ/mol; see Supporting Information, Figure S8 and Tables S8–S10). Notably, the rebound process for heme Fe<sup>IV</sup>=O complexes generally has very low activation energies or is barrierless, and this is likely due to  $\pi$  orbitals of the heme moiety perpendicular to the Fe<sup>IV</sup>=O axis, perhaps triggering similar donations as discussed here for the five non-heme oxidants.<sup>[87]</sup> It has been assumed before that the high reactivity of **5** and **2** is related to the orientation of the pyridine rings<sup>[26]</sup> but a DFT-based analysis of the Fe<sup>IV</sup>=O oxidants did not show any notable effect,<sup>[94]</sup> and only the recognition of the significance of the rebound barrier now allows to appreciate the importance this structural effect of the ligand scaffold. Note that the addition of Lewis acids, reported in reactions of ferryl complexes leads to similar effects.<sup>[95,96]</sup>

Our current interpretation of the HAA reactivity order of **1** to **5** (specifically also the difference between the two isomeric bispidine systems **4** and **5**), i.e., the importance of the rebound barrier and the assumption that this is related to  $\pi$ -donation of the supporting ligand, is one possible factor in understanding and tuning the reactivity, and in the series of oxidants studied here, we propose that it is a major factor. The strikingly different reactivities of **4** and **5** have before been assigned to be mainly due to a ligand structure enforced difference of the energy of the  $S=1$  ground state of Fe<sup>IV</sup>=O, while the quintet state, *TS1* and *Int1* had very similar energies for **4** and **5**, i.e., the larger reactivity of **5** was interpreted to be a result of a larger driving force and smaller triplet-quintet gap, resulting in an easier spin crossover.<sup>[34]</sup> This is supported by an earlier DFT study of these systems and a ligand field analysis<sup>[21,34,97]</sup> and qualitative ligand field arguments. The fact that the reactivity pattern does not agree with the spin state energies reported here could be a

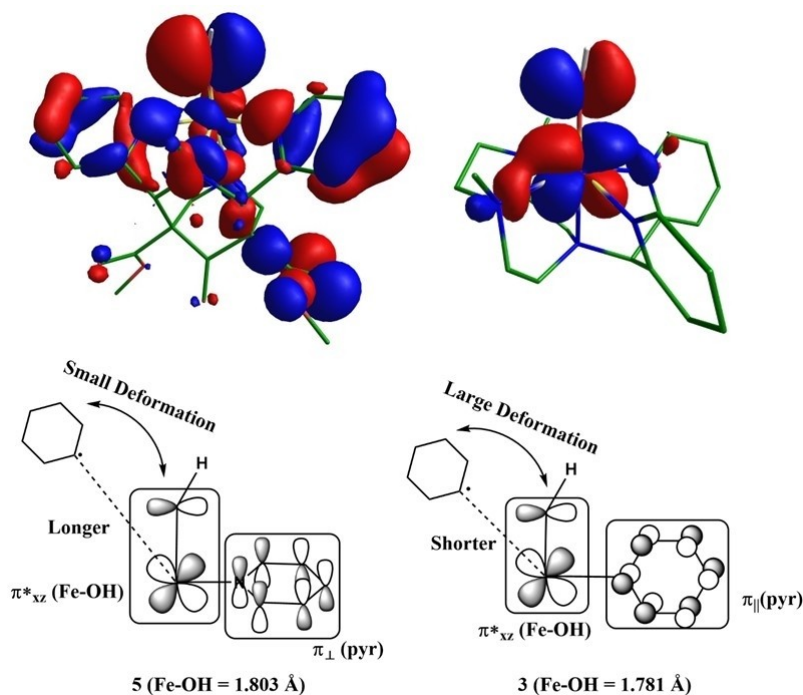


**Figure 3.** Orbital Interaction diagram for the rebound step of complexes **5** and **3** oxidizing cyclohexane. The bond lengths of Fe–OH are given in brackets.

typical artefact of the accuracy of computed energies, see above.

We now quickly turn to the reactivities with cyclohexadiene as substrate. The preferred pathway of the  $\text{Fe}^{\text{III}}\text{-OH}$ /cyclohexadienyl radical intermediate is a fast second PCET step producing the thermodynamically favored aromatic product,<sup>[98]</sup> i.e., the first HAA process is rate limiting. This is in contrast to the reaction with cyclohexane, where HAA is an endergonic process, forming an  $\text{Fe}^{\text{III}}\text{-OH}$ /radical intermediate of significant lifetime, and the barriers of the follow-up reactions therefore are of some importance. For the cyclohexadiene reaction we therefore have only analyzed the first HAA by DFT (see Table 1 and Supporting Information, Table S3). The experimental data indicate that **5** and **2** again are the most efficient oxidants, albeit with inversed order but with only a small difference, and the other three  $\text{Fe}^{\text{IV}}=\text{O}$  complexes are significantly slower (also in reversed order but with quite similar reactivities), and this is well reproduced with the computed energy barriers (see Table 1). It is likely that the differences, primarily between **5**, **2** and the less reactive systems **1**, **3** and **4** is a combination of the driving forces and the quintet-triplet gaps, but this is here not analyzed in detail.

Finally, we compare the computational analyses with additional experimental parameters. Unfortunately, so far there is no experimental evidence for confirming the computed triplet-quintet gaps, which for **5** is predicted to be smaller than for **4**, and for **2** is computed to be very small. Experiments that have been used or proposed to get information on the relative energy of the excited quintet state are field Mössbauer and HF-EPR spectroscopy for obtaining zero-field splitting parameters, ligand field analyses to calculate zero-field splitting parameters and temperature-dependent kinetics, which also depend on spin-orbit coupling matrix elements.<sup>[21,99–101]</sup> Unfortunately, there is no comprehensive data available for the entire series studied here. Rate limiting C–H abstraction is generally probed by kinetic isotope effects (KIE), and data sets of the series of  $\text{Fe}^{\text{IV}}=\text{O}$  complexes **1–5** discussed here and relevant for the oxidation of cyclohexane and cyclohexadiene are available (see Supporting Information, Table S1). For the aromatization of cyclohexadiene, kinetically determined KIEs with dihydroanthracene are relevant (similar type of reaction), and these are in the range of 10 to 30 (with the largest value [31] for **3** and the two bispidine complexes at the lower end [12, 13]), i.e., as expected for rate determining HAT.<sup>[26]</sup> For the cyclohexane hydroxylation, kinetically determined KIEs with PhEt are available for **1** and **2**, and these are very large (27 and 53);<sup>[13]</sup> for **3** there is no reaction with cyclohexane and therefore no KIE, and for **4** and **5**, KIEs with cyclohexane have been measured by product distribution, and these are very small (3.8 and 2.2).<sup>[49]</sup> Here, a note of caution is appropriate: the parameters emerging from product distributions strongly depend on the overall pathway, i.e., (rate determining) HAA involving cyclohexane as well as the formation of the cyclohexanol product, while the kinetic analysis primarily is related to the isotope effect in the HAA alone – according to the importance of the rebound barrier as discussed here, this may need to be corrected, but this is a minor and straightforward task. The problem with the reported

product distribution based values of **4** and **5** is twofold: (i) cage escape significantly reduces the cyclohexanol product formed, and this has been established for the two isomeric oxidants (reaction in the presence of  $\text{O}_2$ ; notably, the amount of cage escape seems to be smaller for **5** than for **4**, in agreement with a smaller rebound barrier of the former), and (ii) the  $\text{Fe}^{\text{IV}}=\text{O}$  species were produced by oxidation of the  $\text{Fe}^{\text{II}}$  precursors with  $\text{H}_2\text{O}_2$ , and this is known to produce OH radicals, which are known to lead to other possible pathways for cyclohexanol formation.<sup>[49,89]</sup>

## Conclusions

From the comprehensive DFT and ab initio (CASSCF/NEVPT2 and DLPNO-CCSD(T)) calculations on the five  $\text{Fe}^{\text{IV}}=\text{O}$  systems with N4py (**1**), bntpen (**2**), py<sub>2</sub>tacn (**3**) and the two isomeric pentadentate bispidines (**4**) and (**5**) and their reactivities towards the oxidation of cyclohexane and cyclohexadiene, in comparison with published experimental data, the main take-home-messages are: (i) For HAA processes in general, the activation barriers for the processes following the generally assumed rate determining hydrogen atom abstraction, i.e. specifically the barrier for the rebound process need to be considered – these may be substantial, and we have shown examples, where the rebound is rate determining. (ii) The effect of pyridine donors perpendicular to the  $\text{Fe}^{\text{IV}}=\text{O}$  axis, which has been known to accelerate HAA processes, is interpreted to be due to donation from the ligand scaffold, leading to a significant elongation of the  $\text{Fe}^{\text{III}}\text{-OH}$  bond and therefore to a reduction of steric strain in the rebound process. Important experiments to confirm (or refute) the current interpretations include (i) the thorough evaluation of redox potentials – a notoriously difficult problem –, in order to get accurate information on the driving force of the HAA step, (ii) accurately determined KIEs with kinetic measurements under identical conditions, in order to determine the relative importance of the initial HAA step, and (iii) experiments to determine the relative size of the triplet-quintet gaps of the  $\text{Fe}^{\text{IV}}=\text{O}$  species, in order to confirm the importance of the electronic structure of the ferryl species in the context of two state reactivity – various spectroscopies (field-Mössbauer, HF-EPR, optical spectroscopy combined with ligand field analyses) and temperature dependent kinetics are possible tools for this.

## Supporting Information Available

Details of computational data as well as molecular geometries and electronic energies of all species discussed in the manuscript are given as Supporting Information.

## Acknowledgements

We thank SERB (SB/SJF/2019-20/12; CRG/2022/001697), New Delhi, India, for the financial support and IIT Bombay for the

high-performance computing facility. SPARC (Ministry of Human Resource Development), India (SPARC/2018-2019/P153/SL) together with DAAD is acknowledged for financial support of PhD student exchange. We are also grateful for support by Heidelberg University and the Alexander von Humboldt society. This study was also conducted within the Max Planck School Matter to Life, supported by the German Federal Ministry of Education and Research (BMBF) in collaboration with the Max Planck Society. The computational resources were provided by the bwForCluster JUSTUS, funded by the Ministry of Science, Research and Arts and the Universities of the State of Baden-Württemberg, Germany, within the framework program bwHPC-C5. Open Access funding enabled and organized by Projekt DEAL.

## Conflict of Interests

The authors declare no conflict of interest.

## Data Availability Statement

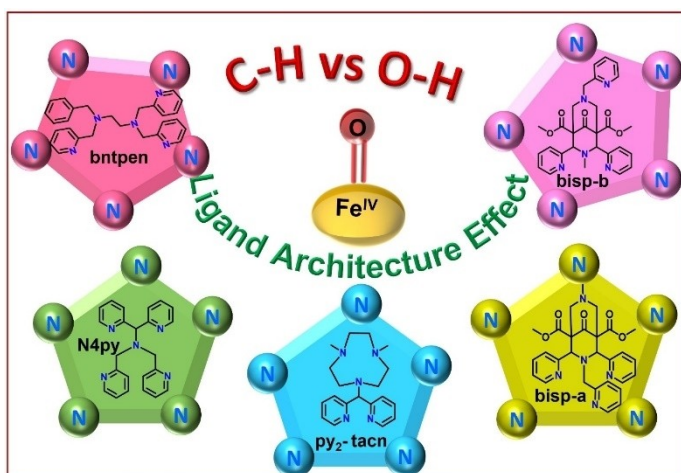
The data that support the findings of this study are available in the supplementary material of this article.

**Keywords:** C–H activation · DFT · DLPNO-CCSD(T) · non-heme iron(IV)oxido · proton coupled electron transfer · quantum-chemical analysis · rebound pathway

- [1] B. E. Eser, E. W. Barr, P. A. Frantom, L. Saleh, J. M. Bollinger, C. Krebs, P. F. Fitzpatrick, *J. Am. Chem. Soc.* **2007**, *129*, 11334–11335.
- [2] A. J. Panay, M. Lee, C. Krebs, J. M. Bollinger, P. F. Fitzpatrick, *Biochemistry* **2011**, *50*, 1928–1933.
- [3] M. L. Matthews, C. M. Krest, E. W. Barr, F. H. Vaillancourt, C. T. Walsh, M. T. Green, C. Krebs, J. M. Bollinger Jr, *Biochemistry* **2009**, *48*, 4331–4343.
- [4] D. P. Galonić, E. W. Barr, C. T. Walsh, J. M. Bollinger, C. Krebs, *Nat. Chem. Biol.* **2007**, *3*, 113–116.
- [5] L. M. Hoffart, E. W. Barr, R. B. Guyer, J. M. Bollinger, C. Krebs, *Proc. Natl. Acad. Sci. U.S.A.* **2006**, *103*, 14738–14743.
- [6] D. A. Proshlyakov, T. F. Henshaw, G. R. Monterosso, M. J. Ryle, R. P. Hausinger, *J. Am. Chem. Soc.* **2004**, *126*, 1022–1023.
- [7] P. J. Riggs-Gelasco, J. C. Price, R. B. Guyer, J. H. Brehm, E. W. Barr, J. M. Bollinger, C. Krebs, *J. Am. Chem. Soc.* **2004**, *126*, 8108–8109.
- [8] J. C. Price, E. W. Barr, B. Tirupati, J. M. Bollinger, C. Krebs, *Biochemistry* **2003**, *42*, 7497–7508.
- [9] J. C. Price, E. W. Barr, T. E. Glass, C. Krebs, J. M. Bollinger, *J. Am. Chem. Soc.* **2003**, *125*, 13008–13009.
- [10] W. Nam, *Acc. Chem. Res.* **2007**, *40*, 522–531.
- [11] M.-H. Baik, B. F. Gherman, R. A. Friesner, S. J. Lippard, *J. Am. Chem. Soc.* **2002**, *124*, 14608–14615.
- [12] F. T. de Oliveira, A. Chanda, D. Banerjee, X. Shan, S. Mondal, L. Que, E. L. Bominaar, E. Münck, T. J. Collins, *Science* **2007**, *315*, 835–838.
- [13] J. Kaizer, E. J. Klinker, N. Y. Oh, J.-U. Rohde, W. J. Song, A. Stubna, J. Kim, E. Muenck, W. Nam, L. Que, Jr., *J. Am. Chem. Soc.* **2004**, *126*, 472–473.
- [14] E. V. Kudrik, P. Afanasiev, L. X. Alvarez, P. Dubourdeaux, M. Clémancey, J.-M. Latour, G. Blondin, D. Bouchu, F. Albrieux, S. E. Nefedov, A. B. Sorokin, *Nat. Chem.* **2012**, *4*, 1024–1029.
- [15] D. Usharani, D. Janardanan, S. Shaik, *J. Am. Chem. Soc.* **2011**, *133*, 176–179.
- [16] R. Kumar, A. Ansari, G. Rajaraman, *Chem. Eur. J.* **2018**, *24*, 6818–6827.
- [17] C. Kupper, B. Mondal, J. Serrano-Plana, I. Klawitter, F. Neese, M. Costas, S. Ye, F. Meyer, *J. Am. Chem. Soc.* **2017**, *139*, 8939–8949.
- [18] S. Meyer, I. Klawitter, S. Demeshko, E. Bill, F. Meyer, *Angew. Chem. Int. Ed.* **2013**, *52*, 901–905.
- [19] S. R. Bell, J. T. Groves, *J. Am. Chem. Soc.* **2009**, *131*, 9640–9641.
- [20] M. Abu-Odeh, K. Bleher, N. Johnee Britto, P. Comba, M. Gast, M. Jaccob, M. Kerscher, S. Krieg, M. Kurth, *Chem. Eur. J.* **2021**, *27*, 11377–11390.
- [21] P. Comba, G. Nunn, F. Scherz, P. H. Walton, *Faraday Discuss.* **2022**, *234*, 232–244.
- [22] M. Ansari, D. Senthilnathan, G. Rajaraman, *Chem. Sci.* **2020**, *11*, 10669–10687.
- [23] K.-B. Cho, H. Hirao, S. Shaik, W. Nam, *Chem. Soc. Rev.* **2016**, *45*, 1197–1210.
- [24] M. G. Evans, M. Polanyi, *Trans. Faraday Soc.* **1936**, *32*, 1333–1360.
- [25] S. P. de Visser, Y.-T. Lin, H. S. Ali, U. K. Bagha, G. Mukherjee, C. V. Sastri, *Coord. Chem. Rev.* **2021**, *439*, 213914.
- [26] D. Wang, K. Ray, M. J. Collins, E. R. Farquhar, J. R. Frisch, L. Gomez, T. A. Jackson, M. Kerscher, A. Waleska, P. Comba, M. Costas, L. Que Jr., *Chem. Sci.* **2013**, *4*, 282–291.
- [27] M. J. Collins, K. Ray, L. Que, *Inorg. Chem.* **2006**, *45*, 8009–8011.
- [28] C. V. Sastri, K. Oh, Y. J. Lee, M. S. Seo, W. Shin, W. Nam, *Angew. Chem. Int. Ed.* **2006**, *45*, 3992–3995.
- [29] Y.-M. Lee, H. Kotani, T. Suenobu, W. Nam, S. Fukuzumi, *J. Am. Chem. Soc.* **2008**, *130*, 434–435.
- [30] P. Comba, S. Fukuzumi, H. Kotani, S. Wunderlich, *Angew. Chem. Int. Ed.* **2010**, *49*, 2622–2625.
- [31] P. Comba, H. Wadepohl, A. Waleska, *Aust. J. Chem.* **2014**, *67*, 398–404.
- [32] D. Bím, L. Rulišek, M. Srnc, *J. Phys. Chem. C* **2018**, *122*, 10773–10782.
- [33] P. Comba, D. Faltermeier, B. Martin, *Z. Anorg. Allg. Chem.* **2020**, *646*, 1839–1845.
- [34] P. Comba, S. Fukuzumi, C. Koke, B. Martin, A.-M. Löhr, J. Straub, *Angew. Chem. Int. Ed.* **2016**, *55*, 11129–11133.
- [35] R. Gupta, A. S. Borovik, *J. Am. Chem. Soc.* **2003**, *125*, 13234–13242.
- [36] S. Shaik, H. Hirao, D. Kumar, *Acc. Chem. Res.* **2007**, *40*, 532–542.
- [37] M. Atanasov, P. Comba, B. Martin, V. Müller, G. Rajaraman, H. Rohwer, S. Wunderlich, *J. Comput. Chem.* **2006**, *27*, 1263–1277.
- [38] P. Comba, in *Comprehensive Coordination Chemistry III* (Eds.: E. C. Constable, G. Parkin, L. Que Jr), Elsevier, Oxford, **2021**, pp. 241–255.
- [39] F. Vlahovic, M. Gruden, S. Stepanovic, M. Swart, *Int. J. Quantum Chem.* **2020**, *120*, e26121.
- [40] P. Verma, Z. Varga, J. E. M. N. Klein, C. J. Cramer, L. Que, D. G. Truhlar, *Phys. Chem. Chem. Phys.* **2017**, *19*, 13049–13069.
- [41] H. Chen, W. Lai, S. Shaik, *J. Phys. Chem. Lett.* **2010**, *1*, 1533–1540.
- [42] C. Geng, S. Ye, F. Neese, *Angew. Chem. Int. Ed.* **2010**, *49*, 5717–5720.
- [43] C. Riplinger, F. Neese, *J. Chem. Phys.* **2013**, *138*, 034106.
- [44] C. Riplinger, B. Sandhoefer, A. Hansen, F. Neese, *J. Chem. Phys.* **2013**, *139*, 134101.
- [45] M. Drosou, C. A. Mitsopoulou, D. A. Pantazis, *J. Chem. Theory Comput.* **2022**, *18*, 3538–3548.
- [46] J. T. Groves, G. A. McClusky, *J. Am. Chem. Soc.* **1976**, *98*, 859–861.
- [47] K.-B. Cho, X. Wu, Y.-M. Lee, Y. H. Kwon, S. Shaik, W. Nam, *J. Am. Chem. Soc.* **2012**, *134*, 20222–20225.
- [48] K. Bleher, P. Comba, D. Faltermeier, A. Gupta, M. Kerscher, S. Krieg, B. Martin, G. Velmurugan, S. Yang, *Chem. Eur. J.* **2022**, *28*, e202103452.
- [49] P. Comba, M. Maurer, P. Vadivelu, *Inorg. Chem.* **2009**, *48*, 10389–10396.
- [50] M. J. Frisch, G. W. Trucks, H. B. Schlegel, G. E. Scuseria, M. A. Robb, J. R. Cheeseman, G. Scalmani, V. Barone, G. A. Petersson, H. Nakatsuji, X. Li, M. Caricato, A. V. Marenich, J. Bloino, B. G. Janesko, R. Gomperts, B. Mennucci, H. P. Hratchian, J. V. Ortiz, A. F. Izmaylov, J. L. Sonnenberg, Williams, F. Ding, F. Lipparini, F. Egidi, J. Goings, B. Peng, A. Petrone, T. Henderson, D. Ranasinghe, V. G. Zakrzewski, J. Gao, N. Rega, G. Zheng, W. Liang, M. Hada, M. Ehara, K. Toyota, R. Fukuda, J. Hasegawa, M. Ishida, T. Nakajima, Y. Honda, O. Kitao, H. Nakai, T. Vreven, K. Throssell, J. A. Montgomery Jr., J. E. Peralta, F. Ogliaro, M. J. Bearpark, J. J. Heyd, E. N. Brothers, K. N. Kudin, V. N. Staroverov, T. A. Keith, R. Kobayashi, J. Normand, K. Raghavachari, A. P. Rendell, J. C. Burant, S. S. Iyengar, J. Tomasi, M. Cossi, J. M. Millam, M. Klene, C. Adamo, R. Cammi, J. W. Ochterski, R. L. Martin, K. Morokuma, O. Farkas, J. B. Foresman, D. J. Fox, Wallingford, CT, **2009**.
- [51] F. Neese, *Wiley Interdiscip. Rev. Comput. Mol. Sci.* **2018**, *8*, e1327.
- [52] C. Lee, W. Yang, R. G. Parr, *Phys. Rev. B* **1988**, *37*, 785–789.
- [53] S. Grimme, *J. Comput. Chem.* **2006**, *27*, 1787–1799.
- [54] J. Tomasi, B. Mennucci, R. Cammi, *Chem. Rev.* **2005**, *105*, 2999–3094.
- [55] B. O. Roos, *Adv. Chem. Phys.* **1987**, *69*, 399–445.

- [56] K. Ruedenberg, L. Cheung, S. Elbert, *Int. J. Quantum Chem.* **1979**, *16*, 1069–1101.
- [57] B. O. Roos, P. R. Taylor, P. E. Sigbahn, *Chem. Phys.* **1980**, *48*, 157–173.
- [58] C. Angeli, S. Borini, M. Cestari, R. Cimraglia, *J. Chem. Phys.* **2004**, *121*, 4043–4049.
- [59] C. Angeli, R. Cimraglia, J.-P. Malrieu, *J. Chem. Phys.* **2002**, *117*, 9138–9153.
- [60] B. Mondal, L. Roy, F. Neese, S. Ye, *Isr. J. Chem.* **2016**, *56*, 763–772.
- [61] S. Ye, F. Neese, *Proc. Natl. Acad. Sci. U.S.A.* **2011**, *108*, 1228–1233.
- [62] M. Reiher, *Theor. Chem. Acc.* **2006**, *116*, 241–252.
- [63] V. G. Chilkuri, F. Neese, *J. Chem. Theory Comput.* **2021**, *17*, 2868–2885.
- [64] S. Evangelisti, J.-P. Daudey, J.-P. Malrieu, *Chem. Phys.* **1983**, *75*, 91–102.
- [65] B. Huron, J. P. Malrieu, P. Rancurel, *J. Chem. Phys.* **1973**, *58*, 5745–5759.
- [66] F. Neese, F. Wennmohs, A. Hansen, U. Becker, *Chem. Phys.* **2009**, *356*, 98–109.
- [67] C. Riplinger, P. Pinski, U. Becker, E. F. Valeev, F. Neese, *J. Chem. Phys.* **2016**, *144*, 024109.
- [68] Y. Guo, C. Riplinger, U. Becker, D. G. Liakos, Y. Minenkov, L. Cavallo, F. Neese, *J. Chem. Phys.* **2018**, *148*, 011101.
- [69] M. Saitow, U. Becker, C. Riplinger, E. F. Valeev, F. Neese, *J. Chem. Phys.* **2017**, *146*, 164105.
- [70] P. Comba, D. Faltermeier, S. Krieg, B. Martin, G. Rajaraman, *Dalton Trans.* **2020**, *49*, 2888–2894.
- [71] K. A. Peterson, D. E. Woon, T. H. Dunning Jr, *J. Chem. Phys.* **1994**, *100*, 7410–7415.
- [72] R. A. Kendall, T. H. Dunning Jr, R. J. Harrison, *J. Chem. Phys.* **1992**, *96*, 6796–6806.
- [73] C. Hättig, F. Weigend, *J. Chem. Phys.* **2000**, *113*, 5154–5161.
- [74] P. E. M. Siegbahn, in *Molecular Modeling and Dynamics of Bioinorganic Systems* (Eds.: L. Banci, P. Comba), Springer Netherlands, Dordrecht, **1997**, pp. 233–253.
- [75] P. E. M. Siegbahn, M. R. A. Blomberg, *Chem. Rev.* **2000**, *100*, 421–438.
- [76] P. Barman, A. K. Vardhaman, B. Martin, S. J. Wörner, C. V. Sastri, P. Comba, *Angew. Chem. Int. Ed.* **2015**, *54*, 2095–2099.
- [77] Q. M. Phung, C. Martín-Fernández, J. N. Harvey, M. Feldt, *J. Chem. Theory Comput.* **2019**, *15*, 4297–4304.
- [78] Q. M. Phung, M. Feldt, J. N. Harvey, K. Pierloot, *J. Chem. Theory Comput.* **2018**, *14*, 2446–2455.
- [79] M. Feldt, Q. M. Phung, *Eur. J. Inorg. Chem.* **2022**, *2022*, e202200014.
- [80] A. Sen, R. Kumar, G. Rajaraman, *Inorganica Chim. Acta* **2022**, *529*, 120654.
- [81] P. Comba, A. F. Sickmüller, *Inorg. Chem.* **1997**, *36*, 4500–4507.
- [82] L. E. Roy, E. Jakubikova, M. G. Guthrie, E. R. Batista, *J. Phys. Chem. A* **2009**, *113*, 6745–6750.
- [83] R. Gupta, A. S. Borovik, *J. Am. Chem. Soc.* **2003**, *125*, 13234–13242.
- [84] C. J. Reed, T. Agapie, *J. Am. Chem. Soc.* **2019**, *141*, 9479–9484.
- [85] M. K. Goetz, J. S. Anderson, *J. Am. Chem. Soc.* **2019**, *141*, 4051–4062.
- [86] S. Shaik, S. Cohen, Y. Wang, H. Chen, D. Kumar, W. Thiel, *Chem. Rev.* **2010**, *110*, 949–1017.
- [87] S. Shaik, D. Kumar, S. P. de Visser, A. Altun, W. Thiel, *Chem. Rev.* **2005**, *105*, 2279–2328.
- [88] J. Pan, E. S. Wenger, M. L. Matthews, C. J. Pollock, M. Bhardwaj, A. J. Kim, B. D. Allen, R. B. Grossman, C. Krebs, J. M. Bollinger, *J. Am. Chem. Soc.* **2019**, *141*, 15153–15165.
- [89] M. R. Bukowski, P. Comba, A. Lienke, C. Limberg, C. Lopez de Laorden, R. Mas-Ballesté, M. Merz, L. Que Jr., *Angew. Chem. Int. Ed.* **2006**, *45*, 3446–3449.
- [90] J. Bautz, P. Comba, C. Lopez de Laorden, M. Menzel, G. Rajaraman, *Angew. Chem. Int. Ed.* **2007**, *46*, 8067–8070.
- [91] P. Comba, M. Maurer, P. Vadivelu, *J. Phys. Chem. (A)* **2008**, *112*, 13028–13036.
- [92] A. Company, I. Prat, J. R. Frisch, R. Mas-Balleste, M. Güell, G. Juhasz, X. Ribas, E. Münck, J. M. Luis, L. Que Jr., M. Costas, *Chem. Eur. J.* **2011**, *17*, 1622–1634.
- [93] Note that, as in the earlier studies,<sup>47</sup> cage escape is (assumed to be) barrierless.
- [94] A. Muruganatham, PhD thesis, Universität Heidelberg **2009**.
- [95] Z. Codolà, L. Gómez, S. T. Kleespies, L. Que Jr, M. Costas, J. Lloret-Fillol, *Nat. Commun.* **2015**, *6*, 5865.
- [96] J. Park, Y. Morimoto, Y.-M. Lee, W. Nam, S. Fukuzumi, *Inorg. Chem.* **2014**, *53*, 3618–3628.
- [97] A. E. Anastasi, P. Comba, J. McGrady, A. Lienke, H. Rohwer, *Inorg. Chem.* **2007**, *46*, 6420–6426.
- [98] D. Janardanan, Y. Wang, P. Schyman, L. Que Jr., S. Shaik, *Angew. Chem. Int. Ed.* **2010**, *49*, 3342–3345.
- [99] J. N. Harvey, *Phys. Chem. Chem. Phys.* **2007**, *9*, 331–343.
- [100] H. Hirao, L. Que Jr., W. Nam, S. Shaik, *Chem. Eur. J.* **2008**, *14*, 1740–1756.
- [101] D. Danovich, S. Shaik, *J. Am. Chem. Soc.* **1997**, *119*, 1773–1786.

Manuscript received: October 9, 2023  
Accepted manuscript online: November 6, 2023  
Version of record online: ■■■



The importance of ligand design to modulate rebound barriers in order to achieve efficient and selective hydrox-

ylation reactions with high-valent  $\text{Fe}^{\text{IV}}=\text{O}$  species is revealed.

R. Kumar, A. Ansari, P. Comba\*, G. Rajaraman\*

1 – 11

Rebound or Cage Escape? The Role of the Rebound Barrier for the Reactivity of Non-Heme High-Valent  $\text{Fe}^{\text{IV}}=\text{O}$  species

